Supplementary Material for PCCP


# States and Migration of Excess Electron in a Pyridinium-Based Room-Temperature Ionic Liquid: An Ab Initio Molecular Dynamics Simulation Exploration

Zhiping Wang,[†] Liang Zhang,[†] Robert I. Cukier,[‡] Yuxiang Bu[1],[†]

*The Center for Modeling & Simulation Chemistry, Institute of Theoretical Chemistry, Shandong University, Jinan, 250100, P. R. China, and Department of Chemistry, Michigan State University, East Lansing, Michigan, 48824-1322*

## Supporting Information

## 1. Geometric details:

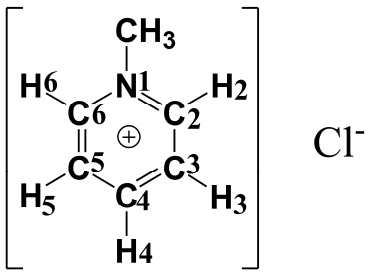


***Figure S1.*** Scheme of 1-methylpyridinium chloride.

[1] *The corresponding author: Dr. Prof. Yuxiang Bu, byx@sdu.edu.cn*
[†] *Shandong University*
[‡] *Michigan State University*

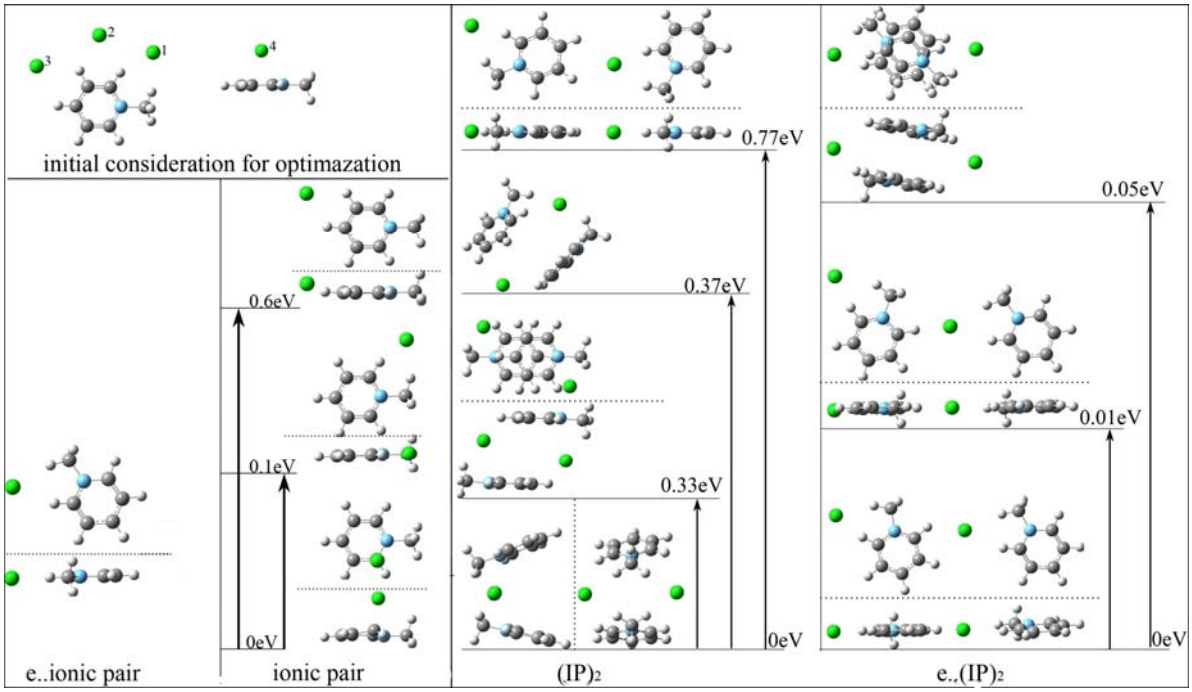


***Figure S2.*** Stationary points of ionic pair $[MePy]^+Cl^-$ and dimeric ionic pairs $([MePy]^+Cl^-)_2$ with and without an excess electron. For $[MePy]^+Cl^-$ and e···$[MePy]^+Cl^-$ four initial configurations were considered with the $Cl^-$ anion located at different points around the cation (as noted with 1-4 ). Three stationary points for the ionic pair were obtained at the B3LYP/6-31+G* level, while only one planar structured configuration was considered for the ionic pair with attachment of an excess electron. The relative energy differences between the other configurations and the most stable ionic pair are labeled in the picture. The most stable configurations of $[MePy]^+Cl^-$ and e···$[MePy]^+Cl^-$ are also confirmed with the MP2 method with the same basis sets; detailed data are given in Table S1.

For the dimeric ionic pairs, initial configurations involving different interaction modes between the ions were inspected too. The stationary points are mainly of two kinds: tiered and planar structures, with the two cations nearly proximal or in the same plane, respectively. The relative energy is also given beside the structures. Considering the poor performance of the DFT method in the description of π–π interactions, the stable tiered structures $([MePy]^+Cl^-)_2$ and e···$([MePy]^+Cl^-)_2$ are also confirmed by the MP2 method using the same basis sets. The comparison of the results from DFT and MP2 calculations is given in Figure S4.

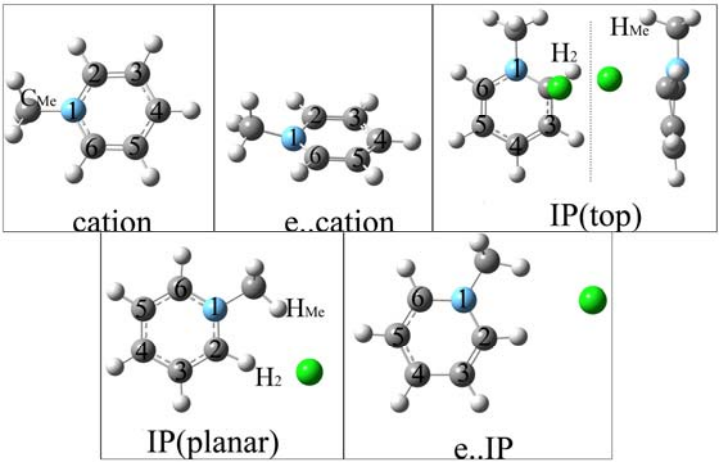


***Figure S3.*** Labeling of $MePy^+$, e···$MePy^+$, $[MePy]^+Cl^-$ (top and planar structures), and e···$[MePy]^+Cl^-$, as involved in Table S1.

***Table S1.*** Selected geometrical parameters (labeled in **Figure S2.**) of the minimum energy configurations fully optimized at the B3LYP /6-31+G* as well as the MP2 /6-31+G* level (DFT value / MP2 value)

| | cation | e···cation | ionic pair(top) | ionic pair (planar) | e···ionic pair |
|---|---|---|---|---|---|
| $C_{Me}$-N(Å) | 1.508/1.485 | 1.451/1.455 | 1.468/1.463 | 1.469/1.489 | 1.454/1.459 |
| $C_2$-N(Å) | 1.361/1.356 | 1.403/1.391 | 1.366/1.387 | 1.356/1.354 | 1.392/1.371 |
| $C_6$-N(Å) | 1.362/1.356 | 1.403/1.391 | 1.367/1.375 | 1.356/1.356 | 1.401/1.391 |
| ∠$C_2$-N- $C_6$(°) | 120.76/121.25 | 118.03/117.83 | 120.79/119.93 | 121.35/122.08 | 119.17/119.62 |
| ϕ $C_{Me}$-N-$C_6$-$C_5$(°) | 178.30/177.66 | 165.23/163.96 | -175.69/176.84 | 179.64/180.00 | 180.00/180.00 |
| $H_2$-Cl | | | 2.565/2.444 | 2.178/2.110 | 2.656/2.539 |
| $H_{Me}$-Cl | | | | 2.382/2.365 | 2.533/2.469 |
| $C_2$-Cl | | | 2.469/2.086 | | |
| ∠ $H_{Me}$-Cl-$H_6$(°) | | | | 58.46/55.77 | 50.24/51.30 |
| ∠N-$C_2$-Cl(°) | | | 103.16/108.66 | | |
| ∠$C_3$-$C_2$-Cl(°) | | | 103.76/106.70 | | |
| $C_2$-N-$C_6$-$C_4$ | | | -8.83/-19.91 | | |

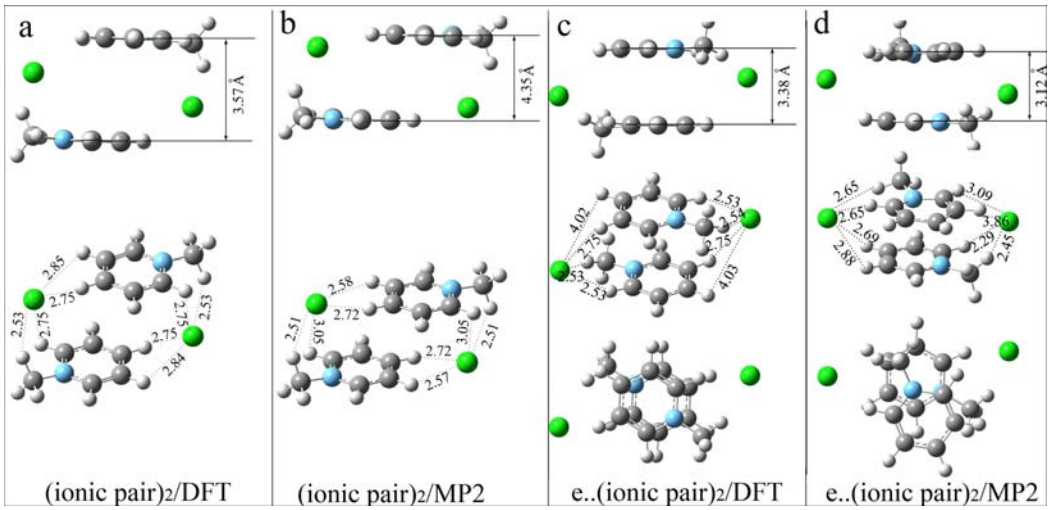


***Figure S4.*** Configurations of the (ionic pair)$_2$ and e···(ionic pair)$_2$ optimized at the B3LYP/6-31+G* (a and c) and MP2/6-31+G*(b and d) levels. Views from different directions are given for clarity. The binding energy of the ionic pair in (ionic pair)$_2$ of a and b are 1.5 eV and 2.0 eV. The vertical electronic affinity energy of the dimeric ionic pair in pictures a and b are 1.1 eV and -0.4 eV.; the vertical electronic detachment energies of the dimeric ionic pair with an excess electron in picture c and d are 2.4 eV and 1.5 eV.

## 2. Relevant Energies and Partial Charge Details:

***Table S2.*** The atomic charges of the constructed models for the molecular dynamics simulations derived from Natural Population Analysis (NPA) of the optimized isolated ionic pairs at B3LYP/6-31+G* level. Configurations of model 1 and 2 come from the top and planar structures of the $[MePy]^+Cl^-$ ionic pair, respectively.

| atoms | model 1 | model 2 |
|---|---|---|
| $N_1$ | -0.377 | -0.315 |
| $C_2$ | 0.125 | 0.083 |
| $H_2$ | 0.237 | 0.307 |
| $C_3$ | -0.207 | -0.249 |
| $H_3$ | 0.231 | 0.280 |
| $C_4$ | -0.139 | -0.164 |
| $H_4$ | 0.216 | 0.264 |
| $C_5$ | -0.139 | -0.164 |
| $H_5$ | 0.223 | 0.270 |
| $C_6$ | 0.086 | 0.055 |
| $H_6$ | 0.208 | 0.256 |
| C-3H | 0.297 | 0.307 |
| Cl | -0.648 | -0.825 |

***Table S3. a)*** The vertical (VDE) and adiabatic (ADE) detachment energies (eV) for **e**···$MePy^+$ and **e**···$[MePy]^+Cl^-$ at the B3LYP/6-31+G* and MP2/6-31+G* levels. The corresponding data for $[dmim]^+Cl^-$ are presented for comparison.

| DFT/MP2 | **e**···$MePy^+$ | **e**···$[MePy]^+Cl^-$ | **e**···$[dmim]^+$ | **e**···$[dmim]^+Cl^-$ |
|---|---|---|---|---|
| VDE(eV) | 5.21/4.64 | 1.98/1.32 | 4.97/4.33 | 1.80/1.19 |
| ADE(eV) | 4.97/4.35 | 1.50/0.86 | 3.94/3.35 | 0.41/-0.11 |
| Deformation energy(eV) | 0.24/0.29 | 0.48/0.46 | 1.03/0.98 | 1.39/1.30 |

***Table S3. b)*** The vertical electronic affinity energy (VAE, in eV) of $MePy^+$, $MePy^+Cl^-$, $[dmim]^+$ and $[dmim]^+Cl^-$.

| DFT/MP2 | $MePy^+$ | $[MePy]^+Cl^-$ /top | $[MePy]^+Cl^-$ /planar | $[dmim]^+$ | $[dmim]^+Cl^-$ /top | $[dmim]^+Cl^-$ /planar |
|---|---|---|---|---|---|---|
| VAE(eV) DFT/MP2 | 4.80/4.19 | 0.31/-1.25 | 1.05/0.74 | 3.27/2.03 | -0.53/-0.93 | -0.38/-0.83 |

***Table S3. c)*** The binding energies (BE, in eV) of $MePy^+$ and **e**..$MePy^+$ with $Cl^-$. The corresponding data for $[dmim]^+$ and **e**···$[dmim]^+$ are presented for comparison

| DFT/MP2 | $[MePy]^+Cl^-$ /top | $[MePy]^+Cl^-$ /planar | **e**···$[MePy]^+Cl^-$ | $[dmim]^+Cl^-$ /top | $[dmim]^+Cl^-$ /planar | **e**···$[dmim]^+Cl^-$ |
|---|---|---|---|---|---|---|
| BE(eV) DFT/MP2 | 3.98/4.07 | 3.86/3.94 | 0.50/0.57 | 3.90/4.06 | 3.93/3.99 | 0.40/0.53 |

***Table S4. a)*** Selected Charges from a Natural Atomic Orbital (NAO) Analysis of e···$[MePy]^+Cl^-$, $[MePy]^+Cl^-$ of both planar and top structures. $\Delta q = q(e\cdots[MePy]^+Cl^-) - q([MePy]^+Cl^-)$

| Atoms | $[MePy]^+Cl^-$(planar) | e···$[MePy]^+Cl^-$ | Δq |
|---|---|---|---|
| *$N_1$* | *-0.315* | *-0.433* | 0.111 |
| *$C_2$* | *0.055* | *-0.057* | *0.153* |
| $H_2$ | 0.256 | 0.185 | 0.107 |
| $C_3$ | -0.269 | -0.235 | 0.026 |
| $H_3$ | 0.270 | 0.191 | 0.048 |
| *$C_4$* | *-0.164* | *-0.325* | *0.204* |
| $H_4$ | 0.264 | 0.186 | 0.037 |
| $C_5$ | -0.249 | -0.267 | 0.038 |
| $H_5$ | 0.280 | 0.201 | 0.030 |
| $C_6$ | 0.083 | 0.020 | 0.076 |
| $H_6$ | 0.307 | 0.258 | -0.040 |
| C-3H | 0.307 | 0.239 | 0.076 |
| *Cl* | *-0.825* | *-0.962* | *0.122* |

| Atoms | $[MePy]^+Cl^-$(top) | e···$[MePy]^+Cl^-$ | Δq |
|---|---|---|---|
| *$N_1$* | -0.377 | *-0.433* | 0.056 |
| *$C_2$* | *0.125* | *-0.057* | *0.182* |
| $H_2$ | 0.237 | 0.185 | 0.052 |
| $C_3$ | -0.207 | -0.235 | 0.028 |
| $H_3$ | 0.231 | 0.191 | 0.04 |
| *$C_4$* | *-0.139* | *-0.325* | *0.186* |
| $H_4$ | 0.216 | 0.186 | 0.03 |
| $C_5$ | -0.254 | -0.267 | 0.013 |
| $H_5$ | 0.223 | 0.201 | 0.022 |
| $C_6$ | 0.086 | 0.020 | 0.066 |
| $H_6$ | 0.208 | 0.258 | -0.05 |
| C-3H | 0.297 | 0.239 | 0.058 |
| *Cl* | *-0.648* | *-0.962* | *0.314* |

***Table S4. b)*** Selected Charges from a Natural Atomic Orbital (NAO) Analysis of $[MePy]^+Cl^-$(top) and ($MePy^+$). $\Delta q = q(MePy^+) - q([MePy]^+Cl^-)$.

| Atoms | $[MePy]^+Cl^-$ | $MePy^+$ | Δq |
|---|---|---|---|
| *$N_1$* | *-0.377* | *-0.319* | *0.057* |
| $C_2$ | 0.125 | 0.116 | -0.009 |
| $H_2$ | 0.237 | 0.236 | -0.001 |
| $C_3$ | -0.207 | -0.198 | 0.009 |
| $H_3$ | 0.231 | 0.253 | 0.021 |
| *$C_4$* | *-0.139* | *-0.083* | *0.057* |
| $H_4$ | 0.216 | 0.245 | 0.028 |
| *$C_5$* | *-0.254* | *-0.197* | *0.057* |
| $H_5$ | 0.223 | 0.253 | 0.029 |
| $C_6$ | 0.086 | 0.115 | 0.029 |
| $H_6$ | 0.208 | 0.236 | 0.028 |
| *C-3H* | *0.297* | *0.343* | *0.046* |
| Cl | -0.648 | | |

***Table S4. C)*** Selected Charges from a Natural Atomic Orbital(NAO) Analysis of $[MePy]^+Cl^-$(top) and ($e\cdots MePy^+$). $\Delta q = q([MePy]^+Cl^-) - q(e\cdots MePy^+)$

| Atoms | MePyCl | $e\cdots MePy^+$ | Δq |
|---|---|---|---|
| $N_1$ | -0.377 | -0.449 | 0.072 |
| *$C_2$* | *0.125* | *-0.020* | *0.145* |
| $H_2$ | 0.237 | 0.194 | 0.043 |
| $C_3$ | -0.207 | -0.229 | 0.022 |
| $H_3$ | 0.231 | 0.208 | 0.023 |
| *$C_4$* | *-0.139* | *-0.293* | *0.154* |
| $H_4$ | 0.216 | 0.200 | 0.016 |
| $C_5$ | -0.254 | -0.229 | -0.025 |
| $H_5$ | 0.223 | 0.208 | 0.015 |
| *$C_6$* | *0.086* | *-0.020* | *0.106* |
| $H_6$ | 0.208 | 0.194 | 0.014 |
| C-3H | 0.297 | 0.235 | 0.062 |
| Cl | -0.648 | | |

## 3. Orbital Analysis of Monomeric and Dimeric Isolated Ionic Pairs

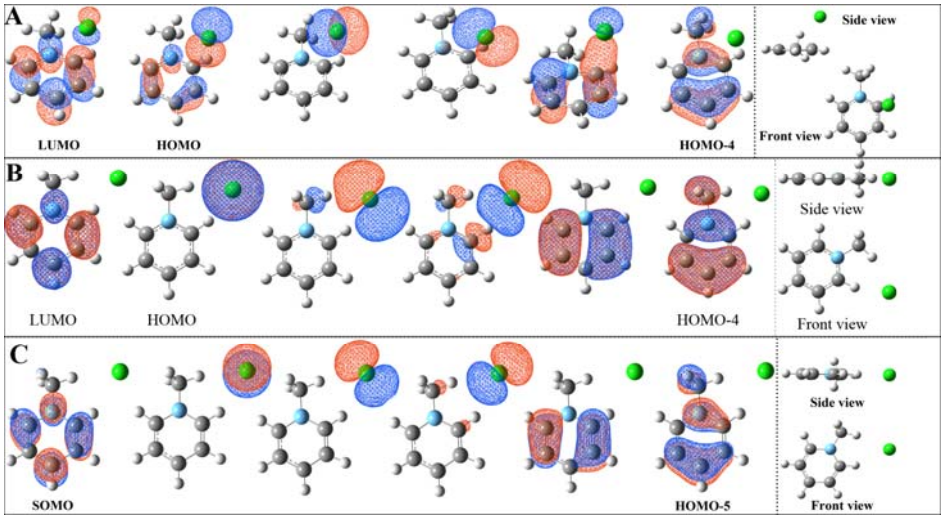


***Figure S5.*** A—the lowest unoccupied molecular orbital (LUMO) and the highest occupied molecular orbitals(HOMO to HOMO-4) of $[MePy]^+Cl^-$(top structure). B—LUMO and HOMO--HOMO-4 of planar $[MePy]^+Cl^-$ ionic pair. C—the singly occupied molecular orbital(SOMO) and HOMO-1 to HOMO-5 of e···$[MePy]^+Cl^-$.

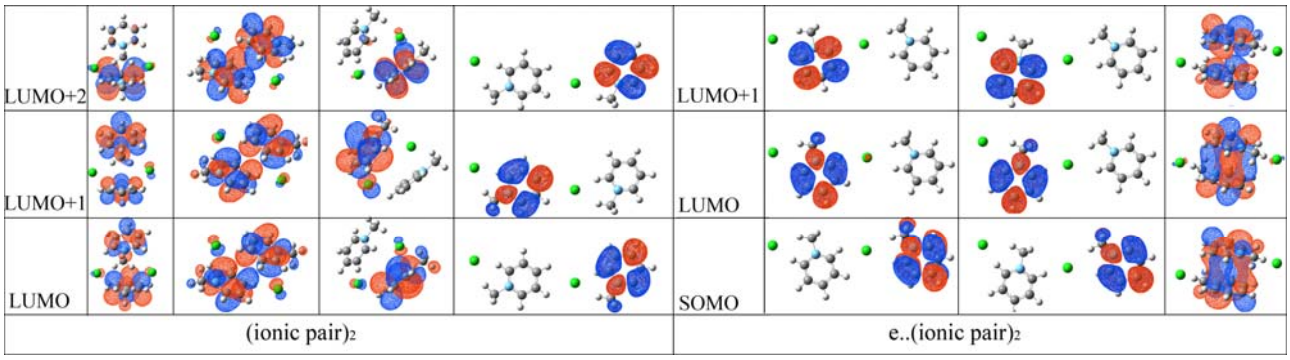


***Figure S6.*** Frontier orbitals plot of the optimized configurations in Figure S2. The LUMO, LUMO+1 and of the neutral dimeric ionic pairs $([MePy]^+Cl^-)_2$ are π∗-type orbitals over one cation or composed by that of two cations. The components of LUMO+2 are also cation π∗-type orbitals which is different from the component of LUMO in the donor ring atoms. With attachment of an excess electron the shapes of the SOMO, LUMO and LUMO+1 orbitals of the e···$([MePy]^+Cl^-)_2$ are similar to the LUMO, LUMO+1 and LUMO+2 of neutral $([MePy]^+Cl^-)_2$.

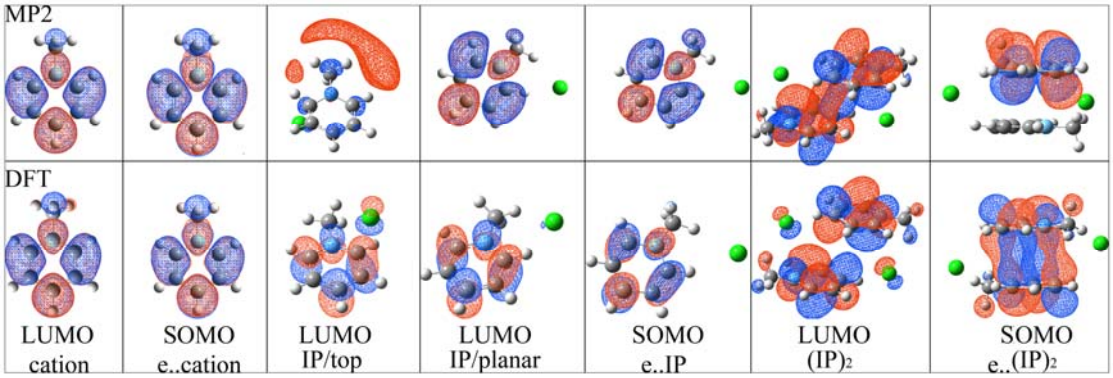


***Figure S7.*** Comparisons between the frontier orbitals plots of various minimum energy configurations optimized at the B3LYP/6-31+G* and MP2/6-31+G* levels. It is shown that, for all those stable configurations, the cation π*-type LUMO is the residence site for an excess electron in both DFT and MP2 results. Note that the LUMO of the top-structured $[MePy]^{+}Cl^{-}$ is a Rydberg orbital while the π*-type orbital is the second lowest unoccupied one and is the favored site for an excess electron as shown by the SOMO of the e···IP, confirming that the C-H moiety cannot bind an excess electron effectively.

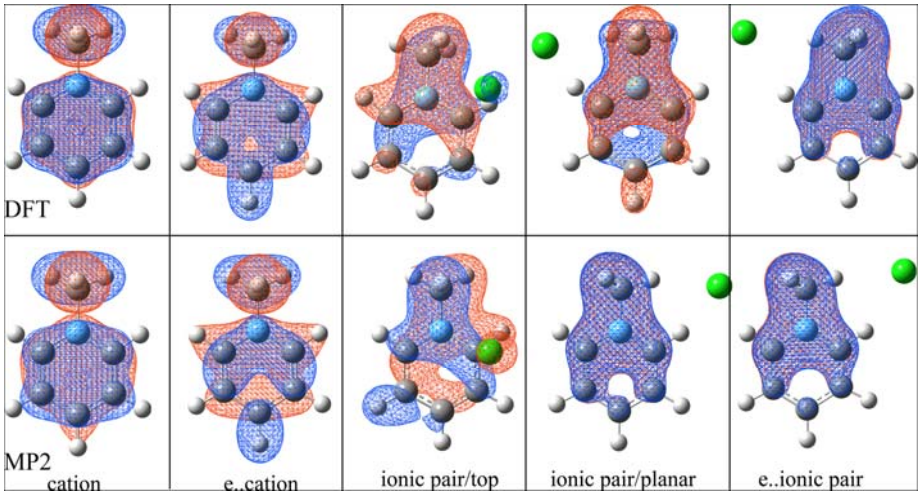


***Figure S8.*** Plots of the cation large π orbitals of the isolated pyridinium cation, e···cation, ionic pairs of both top and planar structure, and e···ionic pair optimized in both DFT and MP2 methods. It is inferred that acceptance of any negative charge from either an excess electron or an anion will destroy the aromatic stability of the cation.

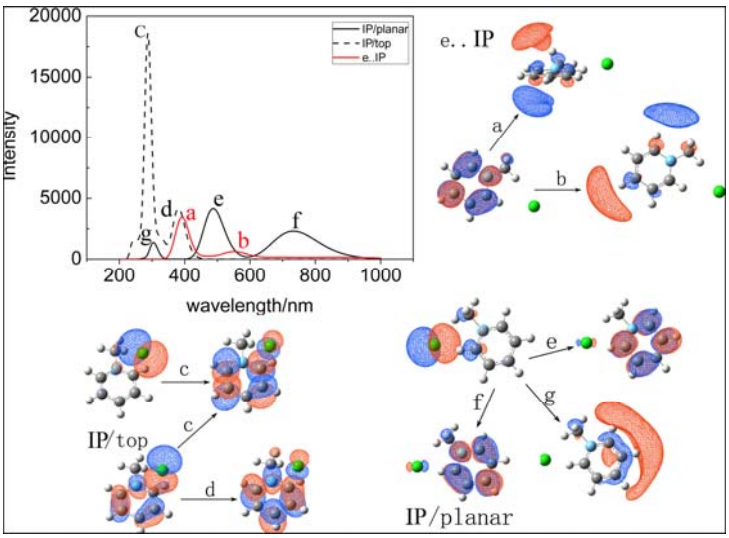


***Figure S9.*** Electronic adsorption spectra of e···$[MePy]^+Cl^-$ (red solid), $[MePy]^+Cl^-$ top (black dashed) and planar (black solid) structures and their corresponding transitions. For the ionic pair of the top structure, the large peak and the weaker one result from electronic transitions from the $p_\pi$ orbitals on the Cl and cation ring atoms to the LUMO+1 and LUMO, respectively. After addition of an excess electron, those two kinds of adsorptions are considerably red-shifted, with a change of transition types and a decrease in transition intensity. That is, the adsorption peaks change into transitions of SOMO (localized at cation moiety) electrons to the p-type (a) and σ-type (b) excited state Rydberg orbitals. The electronic transition seems to occur more readily within the planar structured ionic pair, since two pronounced broad peaks corresponding to electronic transitions from the $p_\pi$ orbitals of the anion to the cation π*-type LUMO+1(e) and LUMO(f) are located in the visual spectrum range. Attachment of an EE only brings about a red shift of the electronic transition from the $p_\pi$ orbitals of $Cl^-$ to the σ-type excited state Rydberg orbitals(g).

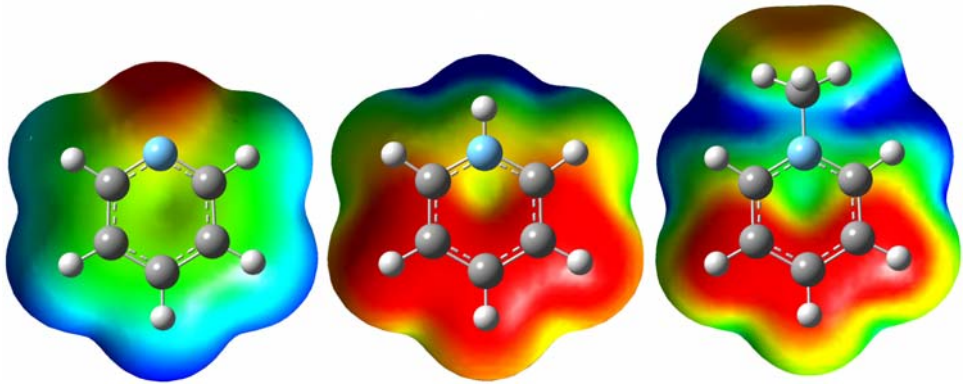

Pyridine $HPy^+$ $MePy^+$

***Figure S10***. Electrostatic potential (ESP) mapped onto the 0.0004 density isosurface for pyridine, protonated pyridine($HPy^+$) and methylpyridinium($MePy^+$). The scale spans -0.04 (red) through 0.0 (green) to +0.03 (blue) for pyridine, -0.15 (red) to 0.2 (blue) for $HPy^+$**,** and -0.14 (red) to 0.17 (blue) for $MePy^+$.

## 4. Structural and orbital details of the bulk ionic liquid.

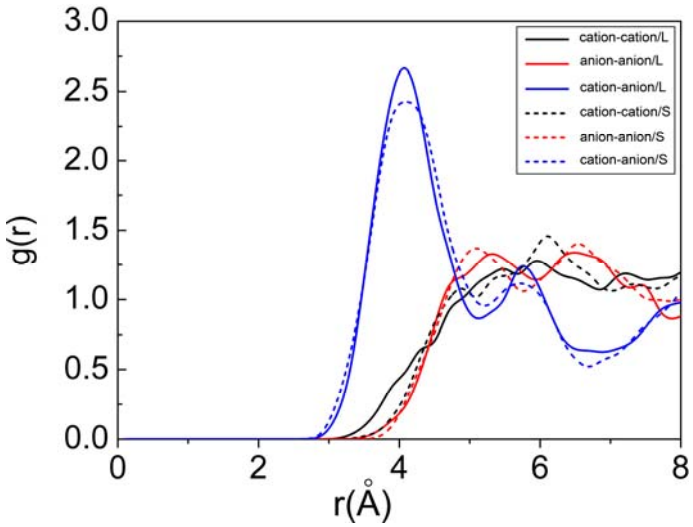


***Figure S11.*** Radial distribution functions $g(r)$ between cation and anion calculated from the trajectory for both large (solid) and small (dashed) systems, considering the N atom as the approximate center of the cation. The good convergence between the solid and dashed curves suggests that these short-range interactions among ions are insensitive to the box size. The location of the pronounced peak in blue and the broader ones in red and black indicate that the average neighboring cation-anion, aion-anion cation-cation distance are 4.1Å, 5.0Å , 5.6Å respectively.

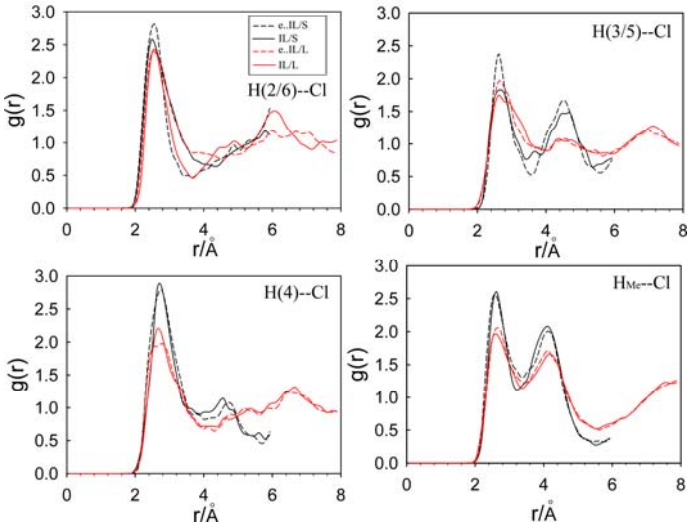


***Figure S12.*** Site-site radial distribution functions between the four kinds of H atoms of the pyridinium cation and the anion calculated on the trajectory from both large (red) and small (black) systems with (dashed) or without (solid) the excess electron. The positions of the peaks from the large and small systems agree well with each other, while the intensity of the g(r) from the small system is stronger than the corresponding ones from the larger one. Comparison of the dashed curves with the solid ones in the same color in every picture indicates the small effect of the EE on the distances between those H atoms and the $Cl^-$ anion.

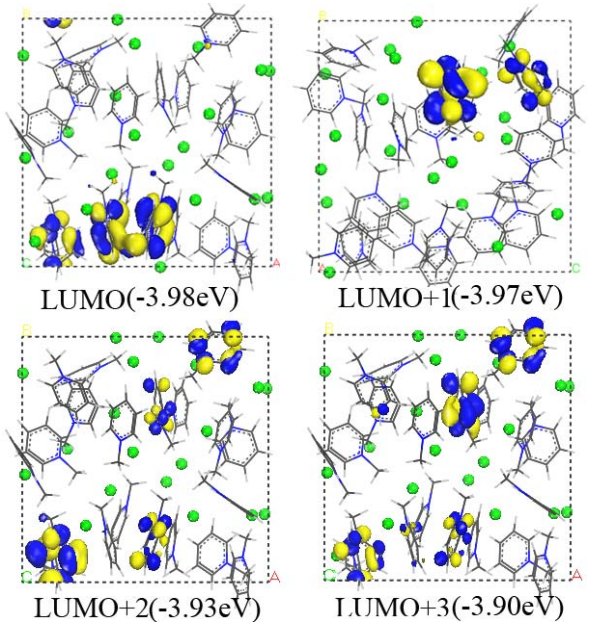


***Figure S13.*** Plots of the lowest unoccupied molecular orbital (LUMO) and the energetically higher ones (LUMO+1---LUMO+3) from a snapshot of neutral ionic liquid system. The orbitals are densely spaced with small differences in energy (noted in parentheses) and all of them are composed of cation π*-type orbitals.

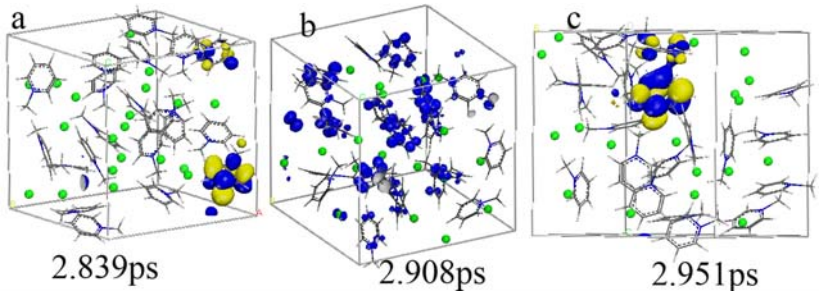


***Figure S14.*** Snapshots from the large box with orbital plots of the simulated system in different electronic states corresponding to an excess electron in 1-methylpyridinium chloride ionic liquid at different times. a and c are snapshots of three localized states at 2.839 and 2.951 ps respectively while b are the spin density distributions corresponding to a certain delocalized state at the intervals of the two localized states, indicating the conversion pathway from one localized state to another. The times below the charts denote the running times immediately after injection of excess electron to the AIMD equilibrated IL.

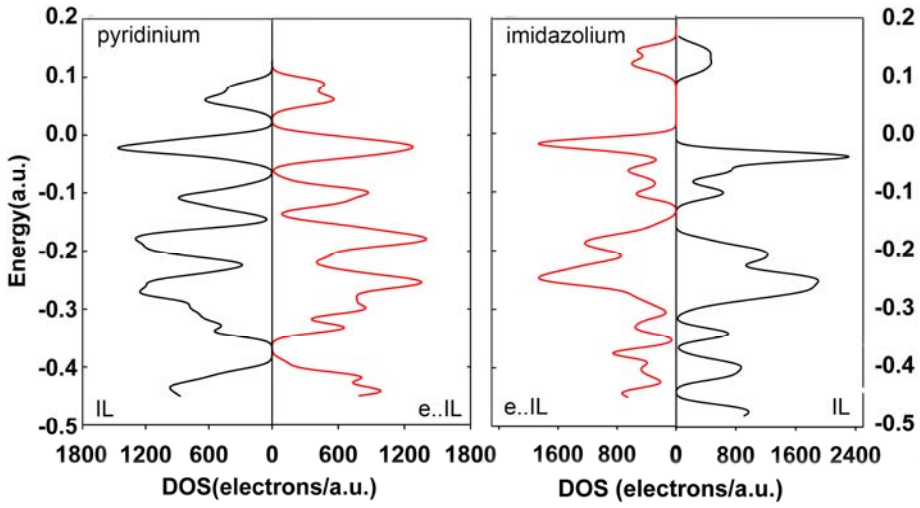


***Figure S15***. Diagram of the density of states (DOS) plots of pyridinium e···IL (red) and IL (black), compared with that of the 1,3-dimethylimidazolium IL. The band gap of the pyridinium IL is obviously smaller than that of the imidazolium IL. The attachment of an EE has a smaller effect on the energy level of the frontier orbitals of the former than the latter. For both kinds of ILs, at the top of the valence band, a weak peak is split out from a strong peak ($Cl^-$ doubly-occupied p orbital set, green) due to EE attachment, which originates from the nearly-degenerate HOMO and HOMO-1 (both π-type) of each cation ring. At the same time, the conduction band is also split into two peaks, contributed by the nearly-degenerate LUMO and LUMO+1 (both $\pi^*$-type) of each cation ring.

***Table S5***. The gaps between the ground state and the first excited state of ten configurations randomly selected from the snapshots of the small box at different times along the e···IL trajectory corresponding to either localized or delocalized electronic states.

| T/ps | 12.320 | 12.368 | 12.515 | 12.627 | 12.904 | 13.004 | 13.073 | 13.863 | 14.186 | 14.850 |
|---|---|---|---|---|---|---|---|---|---|---|
| gap kcal/mol | 25.62 | 29.43 | 33.01 | 19.07 | 25.41 | 30.43 | 12.55 | 9.73 | 18.32 | 3.89 |

The calculations were performed using a semiempirical Hamiltonian method at the ZINDO/INDO/2 level with the VAMP code in Materials Studio to clarify the adiabaticity of the excess electron evolution process in the IL. The RumerCI method was used in the treatment of configuration interaction (CI). 31 CI orbitals with 15 virtual ones were included in the CI calculation to provide accurate results. The electronic states at 12.368 ps, 12.627 ps, 13.073 ps and 13.863 ps are typical delocalized states while those at the remaining times are localized ones. All the calculated gaps are considerably larger than the thermal energy at the room temperature (kT=0.6 kcal/mol), indicating an adiabatic process for the excess electron evolution in this IL (Selloni, A.; Carnevali, P.; Car, R. and Parrinello, M. Phys. Rev. Lett., 1987, 59, 823). Thus the adiabatic assumption does hold in the simulation of the present work.

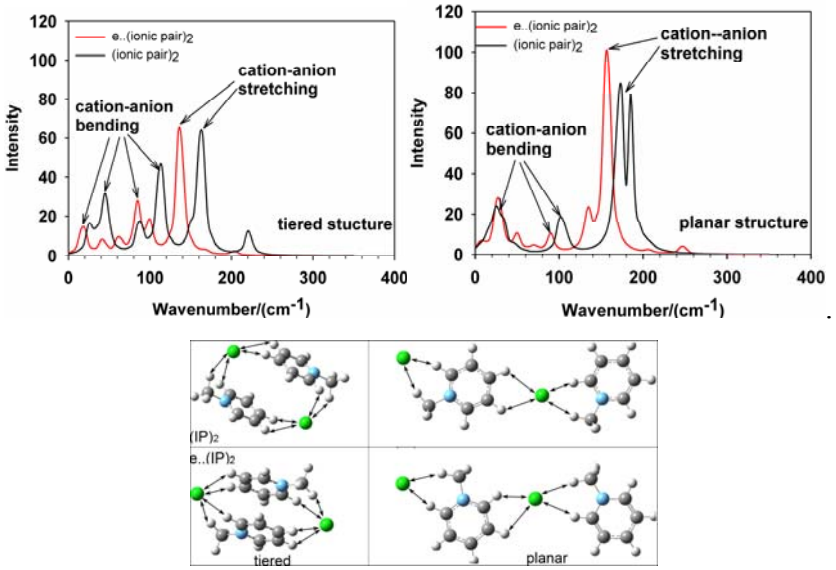


***Figure S16.*** Ab initio calculated far-infrared vibrational spectrum of the $([MePy]^+Cl^-)_2$ (black curve) and **e**···$[MePy]^+Cl^-$ (red curve) of the tiered (left) and planar structures (right). The main peaks in the low-frequency range, denoted by arrows, can be assigned to cation-anion stretching and bending vibrations. The configurations with their vibration modes denoted with arrows are also given for clarity. Note that the attachment of the EE causes significant red-shifts of the C(2)-H(2)···$Cl^-$ vibration peaks.